

Discovery of Local Analogs to JWST's Little Red Dots

RUQIU LIN,^{1,2} ZHEN-YA ZHENG*^{1,2} CHUNYAN JIANG,¹ FANG-TING YUAN,¹ LUIS C. HO,^{3,4} JUNXIAN WANG,⁵ LINHUA JIANG,^{3,4} JAMES E. RHOADS,⁶ SANDEEP MALHOTRA,⁶ L. FELIPE BARRIENTOS,⁷ ISAK WOLD,^{8,9,10} LEOPOLDO INFANTE,¹¹ SHUAI RU ZHU,^{1,2} XIANG JI,¹ AND XIAODAN FU¹

¹Shanghai Astronomical Observatory, Chinese Academy of Sciences, 80 Nandan Road, Shanghai 200030, China

²School of Astronomy and Space Sciences, University of Chinese Academy of Sciences, No. 19A Yuquan Road, Beijing 100049, China

³Kavli Institute for Astronomy and Astrophysics, Peking University, Beijing 100871, China

⁴Department of Astronomy, School of Physics, Peking University, Beijing 100871, China

⁵CAS Key laboratory for Research in Galaxies and Cosmology, Department of Astronomy, University of Science and Technology of China, Hefei, Anhui 230026, China

⁶Astrophysics Science Division, NASA Goddard Space Flight Center, 8800 Greenbelt Road, Greenbelt, MD 20771, USA

⁷Instituto de Astrofísica and Centro de Astroingeniería, Facultad de Física, Pontificia Universidad Católica de Chile, Casilla 306, Santiago 22, Chile

⁸Astrophysics Science Division, Goddard Space Flight Center, Greenbelt, MD 20771, USA

⁹Department of Physics, The Catholic University of America, Washington, DC 20064, USA

¹⁰Center for Research and Exploration in Space Science and Technology, NASA/GSFC, Greenbelt, MD 20771, USA

¹¹Institute of Astrophysics and Center for Astroengineering, Pontificia Universidad Católica de Chile, Santiago 7820436, Chile

ABSTRACT

Recently, the James Webb Space Telescope (JWST) has revealed a new class of high redshift (high- z , $z > 4$) compact galaxies which are red in the rest-frame optical and blue in the rest-frame UV as V-shaped spectral energy distributions (SEDs), referred to as “Little Red Dots” (LRDs). It is very likely that LRDs host obscured broad-line active galactic nuclei (AGNs). In the meanwhile, *Green pea* galaxies (GPs), which are compact dwarf galaxies at low redshift, share various similar properties with high redshift star-forming galaxies. Here we aim to find the connection between the LRDs and GPs hosting broad-line AGNs (BLGPs). With a sample of 19 BLGPs obtained from our previous work, we further identify 7 GPs with V-shaped rest-frame UV-to-optical SEDs that are likely local analogs to LRDs. These V-shaped BLGPs exhibit faint UV absolute magnitudes and sub-Eddington rates similar to those of LRDs. Three of them occupy a similar region as LRDs in the BPT diagram, suggesting they have similar ionization conditions and gas-phase metallicities to LRDs. These similarities suggest that V-shaped BLGPs can be taken as local analogs of high-redshift LRDs. In addition, most (16/19) BLGPs, including 6 V-shaped BLGPs, host over-massive black holes above the local $M_{\text{BH}}-M_*$ relation, making it the first sample of galaxies hosting over-massive black holes at $z < 0.4$. These findings will help us learn more about the formation and co-evolution of early galaxies and black holes.

Keywords: Active galaxies (17) — Compact dwarf galaxies (281) — Supermassive black holes (1663) — Galaxy evolution (594) — High-redshift galaxies (734)

1. INTRODUCTION

Recent spectroscopic observations with the James Webb Space Telescope (JWST) have revealed a population of red compact galaxies at redshift $z > 3$ (Labbe et al. 2023; Akins et al. 2023; Barro et al. 2024; Kocevski

et al. 2024). These “little red dots” (LRDs), which show red colors in the rest-frame optical, but blue colors in the rest-frame UV (“V-shape”), are likely to host obscured active galactic nuclei (AGNs). This is suggested either by their spectral energy distribution (SED) analysis or by the high detection rate of broad-line emission in the LRD sample (Kocevski et al. 2024; Greene et al. 2024). On the other hand, a subset of AGNs identified

Corresponding author: Zhen-Ya Zheng

*email: zhengzy@shao.ac.cn

with broad H α lines just turn out to be LRDs (Matthee et al. 2024).

While the red optical color of LRDs can be attributed to significant dust attenuation in the AGN, the exact physical mechanisms behind their blue UV color remain debated. The UV SED of LRDs can be modeled with either scattered light from an obscured AGN or emission from a young stellar population (Greene et al. 2024). Recent JWST/NIRCam imaging of the rest-frame UV has also revealed host galaxies and off-centered host-galaxy structures in several cases (Kocevski et al. 2024; Iani et al. 2024; Chen et al. 2024). However, the origin of the UV emission requires further investigation with a larger sample.

Additionally, these high-redshift (high- z , $4 < z < 7$) broad-line AGNs are found to host over-massive BHs compared to the local $M_{\text{BH}}-M_*$ relation (Maiolino et al. 2023, 2024; Harikane et al. 2023; Kokorev et al. 2023; Furtak et al. 2024; Pacucci et al. 2023; Yue et al. 2024; Stone et al. 2023; Chen et al. 2024). They can provide valuable insights into the early phase of supermassive black hole (SMBH) growth and the potential roles these faint AGNs may have played in the early Universe, including their influence on cosmic reionization and on their host galaxies.

In the low-redshift (low- z , $z < 0.4$) Universe, luminous star-forming galaxies (SFGs) with strong emission lines and compact morphology, particularly Green Pea galaxies (GPs), are commonly regarded as low- z analogs to early Universe SFGs (Izotov et al. 2011; Cardamone et al. 2009). Pre-JWST studies have highlighted the similarity between low- z compact SFGs and high- z SFGs by comparing various properties, such as oxygen abundances, stellar masses, far-UV absolute magnitudes, star-formation rates, LyC photon production efficiencies, UV continuum slopes, narrow-line ratios, and emission-line equivalent widths (Yang et al. 2016; Izotov et al. 2015, 2021a). Spectroscopic data from HST/COS and FUSE have revealed high escape fractions of both Lyman-continuum (LyC) and Lyman-alpha (Ly α) photons in some GPs, providing a hint on how ionizing photons from galaxies contribute to the cosmic reionization (Leitet et al. 2013; Borthakur et al. 2014; Leitherer et al. 2016; Izotov et al. 2016a,b, 2018, 2021b; Wang et al. 2019; Flury et al. 2022; Jaskot et al. 2019; Henry et al. 2015; Kim et al. 2020; Izotov et al. 2024).

In the JWST era, studies have demonstrated the similarities between those $z \sim 8$ star-forming galaxies and low- z GPs, in terms of gas metallicity, emission line ratios, UV luminosity, and size (Rhoads et al. 2023; Schaefer et al. 2022; Sun et al. 2023; Withers et al. 2023; Brinchmann 2023; Matthee et al. 2023). GPs can be

used to predict the physical properties of high-redshift galaxies and are important for understanding the evolution of galaxies and the processes of star formation and reionization in the early universe.

Given the similarities of a series of properties between GPs and high- z galaxies, we wonder if GPs and LRDs, which are both compact, are similar objects at different redshifts. Since an important feature of LRDs is the high probability of having broad-line AGNs, we will focus on GPs hosting broad-line AGNs. Recently, we have constructed a sample of 59 GPs hosting massive black hole (MBH) candidates with broad H α lines, which is selected from a parent sample of 2190 GPs from LAMOST and SDSS spectroscopic surveys (Lin et al. 2024, hereafter L24). Over 40 percent of these candidates (25/59) are recognized as AGNs via at least one additional method. Furthermore, this sample has systematically more massive black holes than local dwarf galaxies, appearing similar to high- z faint AGNs recently found by JWST (Lin et al. 2024).

In this work, we aim to find the connection between BLGPs and LRDs by searching in our BLGP sample for the most important feature of LRDs, which is the V-shaped UV-to-optical SED. We describe the sample and the method in Section 2. The results are presented in Section 3. In Section 4, we discuss the implications of V-shaped BLGPs and the presence of over-massive BHs in the local Universe. We conclude this study in Section 5. Throughout this paper, we assume the cosmological parameters of $H_0 = 70 \text{ km s}^{-1} \text{ Mpc}^{-1}$, $\Omega_m = 0.3$, and $\Omega_\Lambda = 0.7$.

2. SAMPLE AND METHOD

In this section, we describe the sample and the method for selecting the local analogs to JWST’s LRDs. The initial sample is the GPs with broad H α lines selected by L24, which is briefly introduced in Section 2.1. We then discuss the method of selecting V-shaped BLGPs and their uncertainty in Section 2.2 and Section 2.3, respectively.

2.1. GPs with Broad H α Lines at $z < 0.4$

In L24, we systematically selected 59 GPs with broad H α lines at $z < 0.4$ from a sample of 2190 GPs selected from LAMOST and SDSS spectroscopic surveys. We briefly introduce the selection method and their physical properties below (see L24 for more details).

We search for the broad H α components as the existence of MBHs in GPs. Starting from 2190 GPs’ spectra, we first subtracted the stellar continuum and absorption lines to isolate the pure emission-line spectra. We then fitted [O III] lines using either a single narrow component or a combination of narrow and wide components.

Table 1. Parameters for 19 BLGPs with $\text{FWHM}_{\text{H}\alpha} > 1000 \text{ km s}^{-1}$

Name	z	β_{UV}	β_{opt}	$\log M_{\text{BH}}$ [M_{\odot}]	$\log M_{*}$ [M_{\odot}]	M_{UV}^b [mag]	$\log [\text{N II}]/\text{H}\alpha$	$\log [\text{O III}]/\text{H}\beta$	dataset
(1)	(2)	(3)	(4)	(5)	(6)	(7)	(8)	(9)	(10)
J003515+084859 [†]	0.242	-1.24(0.71)	0.92(0.92)	6.99(0.02)	8.71(0.03)	-19.14(0.32)	-1.68(0.05)	0.78(0.01)	LAMOST/SDSS
J084029+470710	0.042	-1.66(0.13)	-2.89(0.21)	6.41(0.01)	7.76(0.03)	-17.77(0.06)	-2.08(0.03)	0.77(0.01)	SDSS
J085058+303053 [†]	0.280	-1.19(0.55)	0.44(1.18)	6.29(0.18)	8.33(0.08)	-19.22(0.24)	-1.33(0.17)	0.78(0.01)	LAMOST/SDSS
J092359+415736 [†]	0.323	-0.54(0.66)	0.97(0.47)	6.86(0.04)	10.03(0.20)	-18.88(0.30)	-0.56(0.02)	1.10(0.02)	SDSS
J092834+292136 [†]	0.293	-0.39(0.42)	0.21(0.31)	7.76(0.01)	10.02(0.04)	-19.71(0.19)	-1.24(0.03)	0.95(0.01)	SDSS
J093818+411740	0.280	-2.01(0.30)	-0.15(0.54)	6.47(0.23)	8.83(0.04)	-20.74(0.13)	-1.70(0.69)	0.77(0.02)	LAMOST/SDSS
J095618+430727	0.276	-1.39(0.43)	-0.22(0.52)	6.70(0.07)	9.07(0.02)	-20.16(0.19)	-1.14(0.07)	0.55(0.01)	LAMOST
J112615+385817	0.337	0.21(1.09)	0.36(0.39)	7.18(0.07)	10.26(0.13)	-18.29(0.47)	-0.43(0.07)	1.18(0.05)	SDSS
J114840+175633	0.079	-1.37(0.11)	-1.33(0.34)	6.25(0.03)	8.39(0.10)	-18.38(0.04)	-1.96(0.03)	0.85(0.01)	SDSS
J115438+065025 [†]	0.269	-0.45(0.44)	0.65(0.19)	7.62(0.03)	10.08(0.10)	-19.78(0.20)	< -1.22	1.02(0.05)	LAMOST
J120052+331238 [†]	0.303	-1.85(0.98)	1.94(0.33)	8.41(0.03)	9.90(0.03)	-19.42(0.45)	-0.71(0.02)	1.01(0.01)	SDSS
J122245+360218 [†]	0.301	-1.46(0.80)	< 7.43	6.69(0.11)	8.62(0.13)	-19.18(0.35)	< -2.00	0.95(0.02)	SDSS
J124330-024241	0.210	-1.10(0.78)	-4.28(2.34)	6.57(0.08)	8.62(0.34)	-18.43(0.36)	-1.62(0.11)	0.77(0.01)	LAMOST
J140551+515517	0.271	^a	-0.35(0.40)	6.49(0.37)	9.00(0.03)	^a	-0.84(0.16)	0.79(0.06)	LAMOST/SDSS
J142644+271151	0.356	-2.15(0.57)	-0.72(0.41)	7.14(0.04)	9.32(0.29)	-20.00(0.25)	-0.74(0.07)	1.01(0.02)	SDSS
J160550+440540	0.320	^a	1.93(0.31)	7.18(0.03)	9.96(0.08)	^a	-0.73(0.03)	1.03(0.01)	SDSS
J222803+162200	0.226	-1.85(0.30)	-2.34(0.96)	6.24(0.15)	8.56(0.24)	-19.55(0.12)	-1.47(0.04)	0.79(0.01)	LAMOST
J225059+000032	0.081	-1.27(0.33)	-1.84(0.71)	6.17(0.05)	7.96(0.10)	-17.12(0.15)	-1.85(0.05)	0.83(0.03)	SDSS
J225108-003013	0.081	-0.50(0.47)	-1.63(0.48)	6.14(0.05)	7.61(0.31)	-16.55(0.21)	-1.89(0.04)	0.76(0.00)	LAMOST

NOTE. Column (1): Galaxy name. Column (2): Spectroscopic redshift. Column (3): UV continuum slope. Column (4): Optical continuum slope. Column (5): Logarithmic BH masses. Column (6) Logarithmic stellar masses. Column (7): Absolute UV magnitudes directly converted from NUV magnitudes^b. Column (8)-(9): Logarithmic ratio of narrow lines for [N II]/H α and [O III]/H β , respectively. Column (10): spectrum dataset. The values in parentheses are 1σ error.

[†] V-shaped GPs

^a The galaxy is not covered by the *GALEX* UV observation.

^b As the median deviation between the M_{UV} converted from the NUV magnitude and M_{1500} is less than 0.31 mag and negligibly impacts our result, we use the directly converted M_{UV} .

The narrow component represents the star formation and/or AGNs, while the wide component indicates probable outflows. After subtracting the narrow and possible wide components, we examined the presence of the broad H α component. We found 59 GPs with broad H α components which may host MBHs.

We adopt the stellar mass M_{*} of these GPs from L24. The stellar mass was estimated through the SED fitting with **CIGALE** (Noll et al. 2009; Boquien et al. 2019; Burgarella et al. 2005) on broadband photometry with *GALEX*, *SDSS*, and *WISE*. Compared to L24, we update the measurement of BH mass M_{BH} with the modified relation of virial BH mass in Ho & Kim (2015) based on the velocity dispersion and the luminosity of the broad H α component. Following Greene & Ho (2005), we use the conversion of velocity dispersion between H β and H α and the relation of H α luminosity and luminosity at the rest-frame 5100 Å. We adopt the virial coefficient f of 4.47 for H α lines (Woo et al. 2015). This

BH mass estimation has a typical uncertainty of ~ 0.4 dex (Zhuang & Ho 2023). These inferred parameters are listed in Table 1.

2.2. Selecting V-shaped BLGPs

LRDs have three features, which include broad-line AGNs, compact morphologies, and V-shaped SEDs. First, we require a line width cut of the broad H α line as $\text{FWHM}_{\text{H}\alpha, \text{broad}} > 1000 \text{ km s}^{-1}$, which is the selection criterion for high- z faint broad-line AGNs in Mattthee et al. (2023). As a result, there are 19 GPs hosting broad-line AGNs (hereafter BLGPs).

Second, most (14/19) of these BLGPs have compact sizes of $\text{petroRad_r} < 2.5''$ and appear unresolved in SDSS images, although the spatial resolution of SDSS is much poorer than that of JWST.

Finally, following the methodology in Kocevski et al. (2024), we utilize the continuum slopes β (where β is defined by $f_{\lambda} = \lambda^{\beta}$) to identify the V-shaped SED in

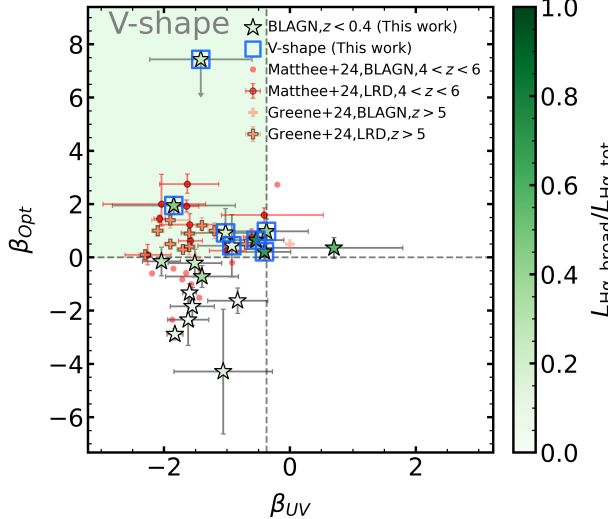


Figure 1. Optical continuum slope β_{opt} vs. UV continuum slope β_{UV} for the GPs hosting broad-line AGNs (stars). The shaded area presents the LRDs selection criteria (Kocevski et al. 2024) with the V-shaped UV-to-optical SEDs. The V-shaped BLGPs are marked on blue squares. The color bar shows the fraction of broad to total H α flux for our BLGP sample. For comparison, we illustrate high- z broad-line AGNs including LRDs reported in Matthee et al. (2023) and Greene et al. (2024).

BLGPs. The criteria used here are $\beta_{\text{UV}} \lesssim -0.37$ for the blue UV continuum slope and $\beta_{\text{opt}} \gtrsim 0$ for the red optical continuum slope, as the shaded region in Figure 1. To determine the UV and optical continuum slopes, we use photometry from the *GALEX* NUV band as well as the SDSS u , i , and z cModel photometry, which are presented in Figure 2. The continuum slope β is defined as the following equation,

$$\beta = -0.4 \frac{m_1 - m_2}{\log(\lambda_1/\lambda_2)} - 2, \quad (1)$$

where the photometric magnitudes (AB) m_1 and m_2 are two continuum bands in the corresponding UV or optical bands. The measurement errors are calculated as $\sigma_\beta = -0.4 \cdot \sqrt{(\sigma_1^2 + \sigma_2^2) / \log(\lambda_1/\lambda_2)}$, where λ_1 and λ_2 represent the effective wavelengths of the bandpasses, and σ_1 and σ_2 are the photometric errors.

For the UV slope, to avoid contamination from the strong Ly α line, we use the NUV and u magnitudes as m_1 and m_2 in Equation 1. Out of 19 BLGPs, 17 are covered by *GALEX* and have NUV detection.

For the optical slope, to avoid contamination from the extreme H β -[O III] emission-line complex which is difficult to remove from the photometry completely, we use the continuum magnitudes in i and z bands as m_1 and m_2 in Equation 1, respectively. Since the H α lines may still contaminate the i -band and z -band photometry at

$0.053 \lesssim z \lesssim 0.245$ and $0.245 \lesssim z \lesssim 0.411$, respectively, we subtract the H α contribution from the photometry to get the continuum magnitudes. The continuum magnitude m_{conti} is then calculated using the equation $m_{\text{conti}} = m_{\text{obs}} + 2.5 \log(\frac{F_{\text{obs}}}{F_{\text{obs}} - F_{\text{line}}})$, where m_{obs} is the observed magnitude and F_{obs} represents the broadband integral flux converted by m_{obs} . The error $\sigma_{m_{\text{conti}}}$ is determined through the error propagation.

2.3. Uncertainty in Selecting V-shaped BLGPs

The identification of V-shaped BLGPs in our sample heavily relies on the UV continuum slopes and the optical continuum slopes. The uncertainty in the optical slope is inherently more complex than that of the UV slope due to the influence of extreme optical emission lines.

The uncertainty in the optical slope arises from the measurement errors in both the emission lines and the continuum. For GP galaxies, the uncertainty in emission-line measurement is generally negligible as these lines are luminous. In contrast, the continuum is relatively faint, resulting in a large uncertainty when directly measuring the continuum from the spectra. This is also why we prefer to use the line-subtracted broadband magnitudes to estimate the optical slopes.

Another source of uncertainty could be emission-line variability probably caused by supernova explosions, tidal disruption events, or changing-look AGNs (Lin et al. 2022). For instance, the optical slope of J122245+360218 is considered an upper limit because the z -band continuum, after subtracting the emission line, appears significantly higher than the corresponding spectra (see Figure 2). The i -band magnitude in the spectrum matches the photometric magnitude, indicating no substantial continuum variability but only emission-line variability between the imaging and spectroscopic observing epochs, which were separated by about 330 days. In addition, this 330-day time lag is insufficient to rule out the possibility of a supernova explosion (Yang et al. 2023; Wang et al. 2024). More recently, the optical variability was also seen in LRDs (Zhang et al. 2024). Despite these uncertainties, we retain this source as its photometry and optical spectrum profile closely match those of the LRD, JADES 10013704 (see the comparison in Figure 2).

3. RESULTS

3.1. V-shaped BLGPs: Local Analogs to LRDs

Based on the broad H α line width and the continuum slope criteria, we identify 7 V-shaped BLGPs as local analogs to LRDs from a sample of 19 BLGPs.

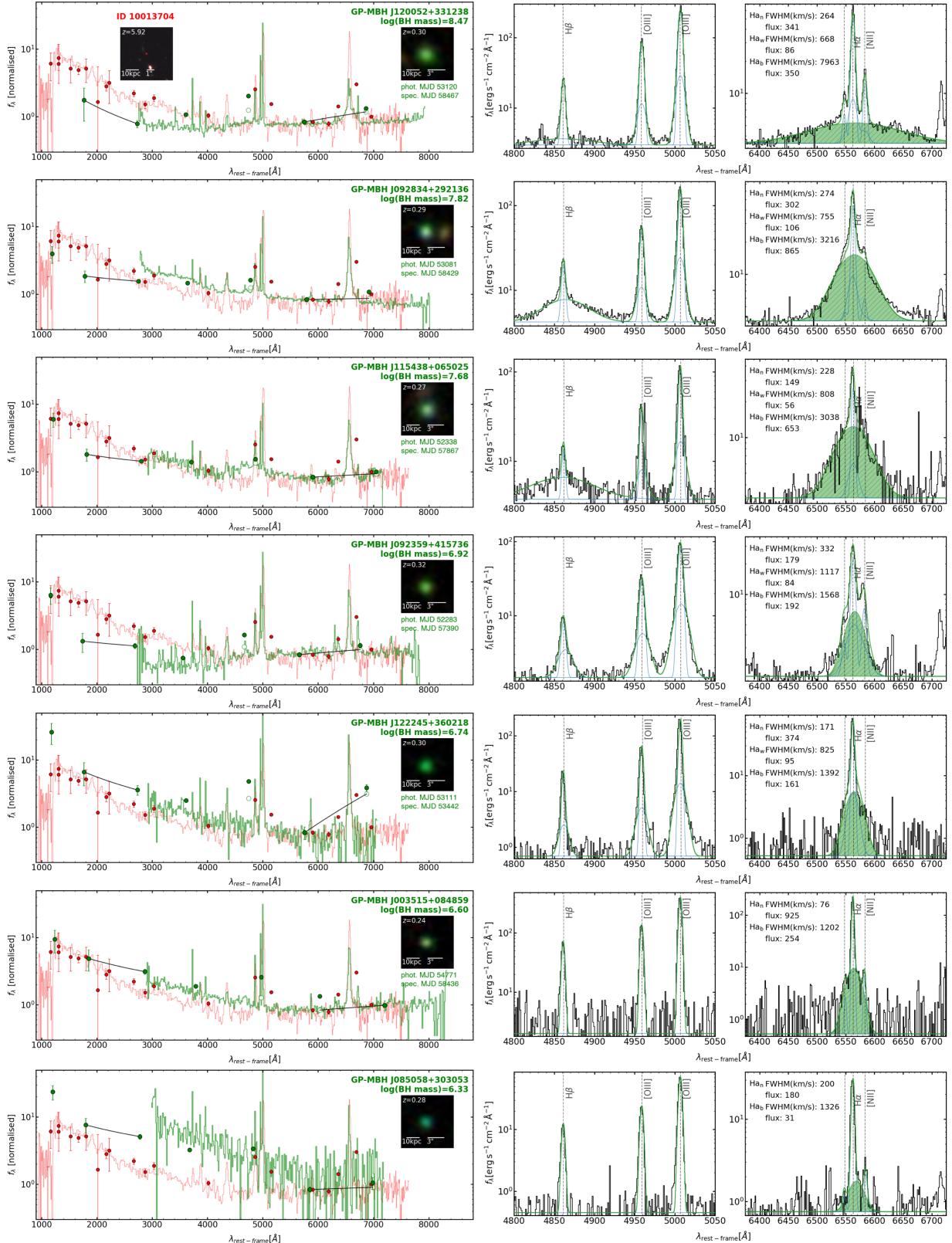


Figure 2. Left column: Comparison of rest-frame UV-to-optical SEDs between the V-shaped BLGPs at $z \sim 0.3$ (green dots) and a LRD (JADES 10013704) at $z = 5.9$ reported in Maiolino et al. (2023) (red dots). The green circles represent the continuum flux after subtracting emission lines. The background red line and the image in the upper left are the NIRSpec/PRISM spectrum and the NIRCam F115W-F200W-F444W color cutout of JADES 10013704. The green line is the SDSS spectra for each V-shaped BLGP, re-binned to the spectral resolution of NIRSpec/PRISM resolution. All photometries and spectra are normalized at rest-frame 5800 Å. For each V-shaped BLGP, the SDSS *gri* color cutout is also illustrated in the upper right of the corresponding subfigure. The observing dates of the image and spectra for each V-shaped BLGP are also labeled. Right column: Emission-line measurement for the V-shaped BLGPs. The black, blue, and green lines are the observed spectra, the narrow (or plus wide) components, and the composite spectra. The green shade is the broad H α component.

In Figure 2, we show the rest-frame SEDs and spectra of these V-shaped BLGPs, as well as those of a typical LRD, JADES 10013704, reported in Maiolino et al. (2023). These local analogs exhibit V-shaped UV-to-optical SEDs and strong emission-line features (especially [O III] and H α) similar to those of JADES 10013704. We also note a likely inverse correlation between the break wavelength of the V-shaped SED and the BH mass in these V-shaped BLGPs (Table 2). This correlation would help us to further constrain many AGN-galaxy hybrid models (e.g., Greene et al. 2024) recently invoked to explain the SED of LRDs.

Additionally, except for V-shaped BLGP with the lowest stellar mass, six others meet the AGN criteria based on the *WISE* mid-infrared colors (Jarrett et al. 2011, also see Table 2). This suggests that they have consistent mid-infrared properties and also align with the scenario of AGNs or starbursts (Figure 12 of Withers et al. 2023).

3.2. Similarity Between V-shaped BLGPs and LRDs

In this section, we present the similarity between V-shaped BLGPs and LRDs in terms of UV absolute magnitude, the relation of optical slopes and BH masses, narrow-line ratio, and Eddington ratios.

V-shaped BLGPs have UV absolute magnitudes ranging from -18.9 to -19.8 mag with a median of -19.2 mag. This is similar to those of LRDs (Matthee et al. 2024; Maiolino et al. 2023; Harikane et al. 2023), placing them in the category of faint AGNs.

Moreover, V-shaped BLGPs have higher M_{BH} and broad-to-total H α luminosity ratio ($L_{\text{H}\alpha,\text{broad}}/L_{\text{H}\alpha,\text{tot}}$) compared to non-V-shaped BLGPs (see Figure 3-a). We find a positive correlation between β_{opt} , M_{BH} , and $L_{\text{H}\alpha,\text{broad}}/L_{\text{H}\alpha,\text{tot}}$, consistent with the samples of Matthee et al. (2023) and Greene et al. (2024). This correlation between β_{opt} and M_{BH} is first found by Matthee et al. (2023) with $M_{\text{BH}} \gtrsim 10^7 M_{\odot}$, and here is extended to $M_{\text{BH}} \sim 10^6 M_{\odot}$ in our sample. This is consistent with that the optical color in these systems is influenced by AGNs.

In Figure 3-b, we compare the locations of V-shaped BLGPs and LRDs in the standard narrow-line diagnostic diagram (BPT diagram, Baldwin et al. 1981). All V-shaped BLGPs, as well as other BLGPs, exhibit high [O III]/H β ratios, indicating a high level of ionization, similar to high- z broad-line AGNs. Three of them have very low [N II]/H α ratios consistent with the LRD JADES 10013704, whereas the other four are more similar to typical low- z AGNs.

To compare the Eddington ratios ($\lambda_{\text{Edd}} \equiv L_{\text{bol}}/L_{\text{Edd}}$, where $L_{\text{Edd}} = 1.26 \times 10^{38} M_{\text{BH}}/M_{\odot}$) between V-shaped

BLGPs and LRDs, we estimate the bolometric luminosity L_{bol} utilizing the empirical relation of $L_{5100} = (\frac{L_{\text{H}\alpha,\text{broad}}}{5.25 \times 10^{42}})^{\frac{1}{1.157}} \times 10^{44} \text{ erg s}^{-1}$ (Greene & Ho 2005) and $L_{\text{bol}} = 9.8 L_{5100}$ (McLure & Dunlop 2004, also see Greene & Ho 2007). In Figure 3-c, we present the L_{bol} vs. M_{BH} diagram. V-shaped BLGPs systematically have lower bolometric luminosities and smaller BH masses than LRDs, while most exhibit an Eddington ratio of approximately 0.1, similar to that of LRDs (Greene et al. 2020; Maiolino et al. 2023; Harikane et al. 2023; Kocevski et al. 2023).

Overall, V-shaped BLGPs exhibit similar properties to LRDs, not only in terms of broad-line widths and rest-frame UV-to-optical SEDs but also regarding rest-frame UV absolute magnitudes, the relation of optical slopes and BH masses, narrow-line diagnostics, and Eddington ratios. These similarities make V-shaped BLGPs a valuable local sample to study the early growth and evolution of SMBHs in a local context.

4. DISCUSSION

4.1. Implication of V-shaped BLGPs

In this section, we discuss the implication of V-shaped BLGPs in revealing the physical origin of the UV emission of LRDs. To distinguish between different physical origins of UV emission—whether from star formation or AGN scattered light—we can use UV emission lines (such as [Mg II], C III], and C IV) or UV morphology. However, it remains a challenge for the high- z sample, as higher-resolution spectra or deeper imaging with JWST in the rest-frame UV band is needed (e.g., Greene et al. 2024; Matthee et al. 2024).

In contrast, for low- z V-shaped BLGPs, obtaining the UV observations with high sensitivity and high spatial resolution is more feasible. With this sample of V-shaped BLGPs, we can further determine the exact physical origin of the UV emission. For instance, the most massive two V-shaped BLGPs, J120052+331238 and J092834+292136, exhibit significant Mg II lines (See Figure 2 and Table 2), implying that its UV emission originates from scattered light of the center AGN. In the future, a solid conclusion will be made by utilizing deep UV spectroscopic and imaging observations with high spatial resolution taken from instruments such as HST/COS.

4.2. Low- z Over-massive BHs

Over-massive BHs have been frequently observed in high- z broad-line AGNs and widely discussed in the literature (Maiolino et al. 2023; Harikane et al. 2023; Kokorev et al. 2023; Übler et al. 2023). As shown in Figure 4, 16 BLGPs (including 6 V-shaped BLGPs) lay above the

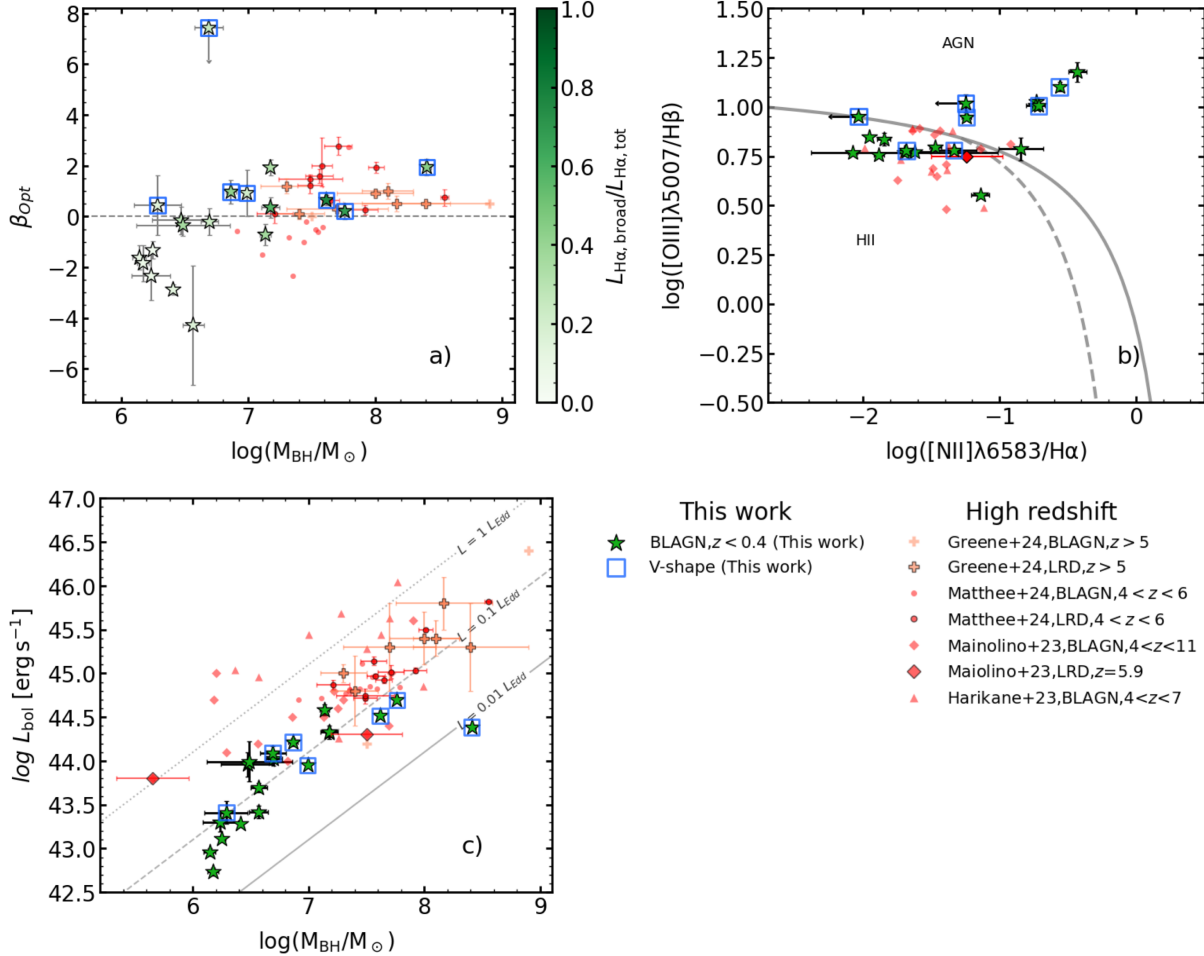


Figure 3. Panel a: Optical continuum slope vs. BH mass for BLGPs (stars). For comparison, we illustrate high- z broad-line AGNs including LRDs reported in Maiolino et al. (2023), Matthee et al. (2023), Greene et al. (2024), and Harikane et al. (2023), if available. Panel b: BPT diagram. The classification lines follow Kewley et al. (2001) (solid line) and Kauffmann et al. (2003) (dashed line), also seen in Kewley et al. (2006). Here we also mark JADES 10013704 in big diamonds. Panel c: Bolometric luminosity vs. BH mass. The grey lines indicate Eddington ratios of $\lambda_{Edd} = 1, 0.1, 0.01$.

local $M_{BH}-M_*$ relation (Greene et al. 2020; Zhuang & Ho 2023) more than 1σ , indicating the presence of over-massive BHs. These galaxies distribute similarly in the $M_{BH}-M_*$ diagram with the broad-line AGNs (including LRDs) reported in literature (Maiolino et al. 2023; Harikane et al. 2023; Kocevski et al. 2023). Compared with the measurement of Chen et al. (2024), who decomposed the AGN and host emission with multi-band images of LRDs and obtained clear stellar mass measurements, BLGPs have lower BH masses and lower M_{BH}/M_* which are up to 0.04. Our sample of over-massive BHs at $z < 0.4$ is rare and the first at such low redshifts. That challenges our current understanding of the BH formation.

The mechanisms behind the formation and evolution of these over-massive BHs remain uncertain. In the early Universe, it involves seeding models such as Eddington or super-Eddington accretion of light seeds, or

Eddington-limit accretion of heavy seeds (Pacucci et al. 2023). In the local Universe, the formation of such BHs may be more complex due to the additional processes they undergo over time. Despite these complexities, the similarity of our BLGPs and high- z broad-line AGNs suggests that they have probably experienced a similar evolutionary track. One possible mechanism for the formation of our sample is they are leftover black hole seeds, that they are formed from the early Universe, and have not experienced significant merging or evolution (Mezcua 2017).

Alternately, BH coalescence and feedback can be another mechanism for the formation of low- z BLGPs. Previous studies investigated over-massive BH samples at $0.4 < z < 3$ (Mezcua et al. 2023, 2024). They suggest that over-massive BHs may form through mergers and efficient gas accretion, with feedback processes suppressing star formation. This scenario supports the existence

Table 2. Properties of V-shaped BLGPs Ordered by BH Masses

Name	Mid-IR ^a AGN	BPT ^a type	Mg II	Break λ_{rest} [Å]	$\log M_{\text{BH}}$ [M_{\odot}]	$\log M_{*}$ [M_{\odot}]
(1)	(2)	(3)	(4)	(5)	(6)	(7)
J120052+331238	1	AGN	1	2800	8.41	9.90
J092834+292136	1	AGN	1	2000-3600	7.76	10.02
J115438+065025	1	AGN	0	2000-3600	7.62	10.08
J092359+415736	1	AGN	–	3000	6.86	10.03
J122245+360218	1	SF-Seyfert	–	4300	6.69	8.62
J003515+084859	1	SF	–	5300	6.99	8.71
J085058+303053	0	SF-Seyfert	–	6000	6.29	8.33

NOTE. Column (1): Galaxy name. Column (2): Classification based on the *WISE* mid-infrared color-color diagram (Jarrett et al. 2011), where 1 indicates an AGN and 0 indicates a non-AGN. Column (3): BPT classification. Column (4): Presence of the Mg II $\lambda 2800$ line, where 1, 0, and – indicate its presence, the absence, and that it is outside the spectral coverage, respectively. Column (5): Break wavelength at the division between the blue and red sides, which are inspected visually. Column (6): BH mass. Column (7): Galaxy stellar mass. We note that these 7 V-shaped BLGPs are ordered by their BH masses.

^a Classification from L24.

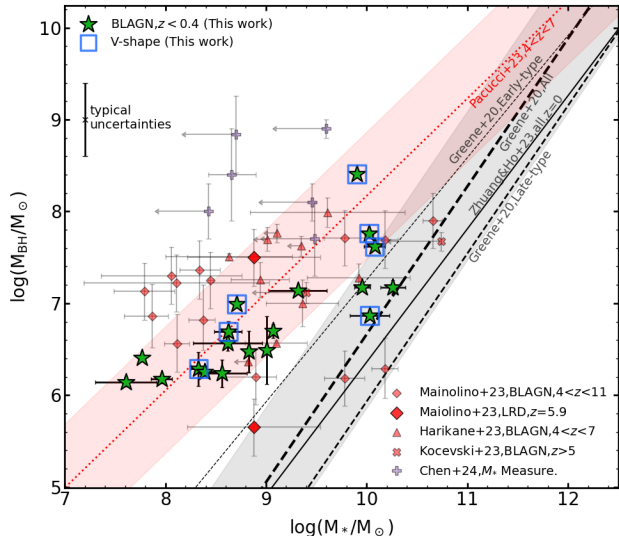


Figure 4. M_{BH} vs. M_{*} diagram. For comparison, we illustrate high- z broad-line AGNs including LRDs reported in Maiolino et al. (2023), Kocevski et al. (2023), and Harikane et al. (2023). Six LRDs with stellar mass measurements derived by Chen et al. (2024) are also plotted. The black dashed lines illustrate the local $M_{\text{BH}}-M_{*}$ relations derived for all, early-type, and late-type galaxies (Greene et al. 2020). The solid line represents the scaling relation for AGNs evolved to $z=0$ (Zhuang & Ho 2023). The dotted line represents the $M_{\text{BH}}-M_{*}$ relation at $4 < z < 7$ (Pacucci et al. 2023). Shaded areas show 1σ intrinsic scatters.

of over-massive BHs at $z < 3$, although they are expected to evolve to align with the local scaling relation by $z \sim 0$. The presence of over-massive BHs in the local Universe may imply that center BH significantly regulates the star formation in these systems.

We note that this phenomenon of having over-massive BHs for BLGPs is unlikely to result from the underestimation of stellar masses in their host galaxies. Here we calculate the stellar masses for broad-line AGNs in Maiolino et al. (2023) with our method. The median and average offsets from their results are 0.10 dex and -0.07 dex, respectively, indicating that our method has no systematic deviation from theirs.

5. CONCLUSION

Given the similarities in physical properties between GPs and high- z SFGs, we investigated whether BLGPs could be local analogs to LRDs that also host broad-line AGNs. By comparing the rest-UV and rest-optical continuum slopes of 19 BLGPs with those of LRDs, we identified 7 BLGPs likely to be local analogs to LRDs.

These V-shaped BLGPs exhibit faint rest-UV absolute magnitudes and sub-Eddington accretion rates similar to those of LRDs. Three of them occupy star-formation locus in the BPT diagram, suggesting comparable ionized conditions and gas-phase metallicities similar to LRDs. Most V-shaped BLGPs (6/7) host BHs more massive than the local scaling relation of dwarf galaxies, which is similar to LRDs.

In general, V-shaped BLGPs and LRDs are similar populations at different redshifts, sharing similarities in rest-frame UV-to-optical SEDs, UV absolute magnitudes, narrow-line ratios, Eddington ratios, and the $M_{\text{BH}}-M_{*}$ relation.

Additionally, we find that most (16/19) BLGPs host over-massive BHs with masses above the local relation by more than 1σ and distribute similarly to high- z broad-line AGNs in the $M_{\text{BH}}-M_{*}$ diagram. This over-

massive BH sample is rare and the first sample at $z < 0.4$, implying the challenge of understanding the BH formation.

GPs provide a local subsample that can be considered analogs to LRDs and high- z broad-line AGNs. Combined with follow-up observation including spectroscopic and imaging observations with high sensitivity and high spatial resolution in the UV and optical bands, this V-shaped BLGP sample can help to address several unclear questions for LRDs, such as the UV emission origin.

ACKNOWLEDGMENTS

This work is supported by National Key R&D Program of China No.2022YFF0503402. ZYZ acknowledges the support by the China-Chile Joint Research Fund (CCJRF No. 1906). We also acknowledge the science research grants from the China Manned Space Project, especially, NO. CMS-CSST-2021-A04, CMS-CSST-2021-A07. LCH acknowledges National Science Foundation of China (11721303, 11991052, 12011540375, 12233001), the National Key R&D Program of China (2022YFF0503401), and the China Manned Space Project (CMS-CSST-2021-A04, CMS-CSST-2021-A06). LFB acknowledges the support of ANID BASAL project FB210003 and FONDECYT project 1230231.

Guoshoujing Telescope (the Large Sky Area Multi-Object Fiber Spectroscopic Telescope LAMOST) is a National Major Scientific Project built by the Chinese Academy of Sciences. Funding for the project has been provided by the National Development and Reform Commission. LAMOST is operated and managed by the National Astronomical Observatories, Chinese Academy of Sciences.

Funding for the Sloan Digital Sky Survey V has been provided by the Alfred P. Sloan Foundation, the Heising-Simons Foundation, the National Science Foundation, and the Participating Institutions. SDSS acknowledges support and resources from the Center for High-Performance Computing at the University of Utah. The SDSS web site is www.sdss.org. SDSS is managed by the Astrophysical Research Consortium for the Participating Institutions of the SDSS Collaboration, including the Carnegie Institution for Science, Chilean National Time Allocation Committee (CNTAC) ratified researchers, the Gotham Participation Group, Harvard University, Heidelberg University, The Johns Hopkins University, L'Ecole polytechnique fédérale de Lausanne (EPFL), Leibniz-Institut für Astrophysik Potsdam (AIP), Max-Planck-Institut für Astronomie (MPIA Heidelberg), Max-Planck-Institut für Extraterrestrische Physik (MPE), Nanjing University, National Astronomical Observatories of China (NAOC), New Mexico State University, The Ohio State University, Pennsylvania State University, Smithsonian Astrophysical Observatory, Space Telescope Science Institute (STScI), the Stellar Astrophysics Participation Group, Universidad Nacional Autónoma de México, University of Arizona, University of Colorado Boulder, University of Illinois at Urbana-Champaign, University of Toronto, University of Utah, University of Virginia, Yale University, and Yunnan University. This research has made use of data obtained from the Chandra Source Catalog, provided by the Chandra X-ray Center (CXC) as part of the Chandra Data Archive.

Facilities: SDSS, LAMOST, GALEX, WISE

Software: astropy ([Astropy Collaboration et al. 2013, 2018](https://astropy.org))

REFERENCES

Akins, H. B., Casey, C. M., Allen, N., et al. 2023, ApJ, 956, 61, doi: [10.3847/1538-4357/acef21](https://doi.org/10.3847/1538-4357/acef21)

Astropy Collaboration, Robitaille, T. P., Tollerud, E. J., et al. 2013, A&A, 558, A33, doi: [10.1051/0004-6361/201322068](https://doi.org/10.1051/0004-6361/201322068)

Astropy Collaboration, Price-Whelan, A. M., Sipőcz, B. M., et al. 2018, AJ, 156, 123, doi: [10.3847/1538-3881/aabc4f](https://doi.org/10.3847/1538-3881/aabc4f)

Baldwin, J. A., Phillips, M. M., & Terlevich, R. 1981, PASP, 93, 5, doi: [10.1086/130766](https://doi.org/10.1086/130766)

Barro, G., Pérez-González, P. G., Kocevski, D. D., et al. 2024, ApJ, 963, 128, doi: [10.3847/1538-4357/ad167e](https://doi.org/10.3847/1538-4357/ad167e)

Boquien, M., Burgarella, D., Roehlly, Y., et al. 2019, A&A, 622, A103, doi: [10.1051/0004-6361/201834156](https://doi.org/10.1051/0004-6361/201834156)

Borthakur, S., Heckman, T. M., Leitherer, C., & Overzier, R. A. 2014, Science, 346, 216, doi: [10.1126/science.1254214](https://doi.org/10.1126/science.1254214)

Brinchmann, J. 2023, MNRAS, 525, 2087, doi: [10.1093/mnras/stad1704](https://doi.org/10.1093/mnras/stad1704)

Burgarella, D., Buat, V., & Iglesias-Páramo, J. 2005, MNRAS, 360, 1413, doi: [10.1111/j.1365-2966.2005.09131.x](https://doi.org/10.1111/j.1365-2966.2005.09131.x)

Cardamone, C., Schawinski, K., Sarzi, M., et al. 2009, MNRAS, 399, 1191, doi: [10.1111/j.1365-2966.2009.15383.x](https://doi.org/10.1111/j.1365-2966.2009.15383.x)

Chen, C.-H., Ho, L. C., Li, R., & Zhuang, M.-Y. 2024, arXiv e-prints, arXiv:2411.04446, doi: [10.48550/arXiv.2411.04446](https://doi.org/10.48550/arXiv.2411.04446)

Flury, S. R., Jaskot, A. E., Ferguson, H. C., et al. 2022, *ApJS*, 260, 1, doi: [10.3847/1538-4365/ac5331](https://doi.org/10.3847/1538-4365/ac5331)

Furtak, L. J., Labb  , I., Zitrin, A., et al. 2024, *Nature*, 628, 57, doi: [10.1038/s41586-024-07184-8](https://doi.org/10.1038/s41586-024-07184-8)

Greene, J. E., & Ho, L. C. 2005, *ApJ*, 630, 122, doi: [10.1086/431897](https://doi.org/10.1086/431897)

—. 2007, *ApJ*, 667, 131, doi: [10.1086/520497](https://doi.org/10.1086/520497)

Greene, J. E., Strader, J., & Ho, L. C. 2020, *ARA&A*, 58, 257, doi: [10.1146/annurev-astro-032620-021835](https://doi.org/10.1146/annurev-astro-032620-021835)

Greene, J. E., Labbe, I., Goulding, A. D., et al. 2024, *ApJ*, 964, 39, doi: [10.3847/1538-4357/ad1e5f](https://doi.org/10.3847/1538-4357/ad1e5f)

Harikane, Y., Zhang, Y., Nakajima, K., et al. 2023, *ApJ*, 959, 39, doi: [10.3847/1538-4357/ad029e](https://doi.org/10.3847/1538-4357/ad029e)

Henry, A., Scarlata, C., Martin, C. L., & Erb, D. 2015, *ApJ*, 809, 19, doi: [10.1088/0004-637X/809/1/19](https://doi.org/10.1088/0004-637X/809/1/19)

Ho, L. C., & Kim, M. 2015, *ApJ*, 809, 123, doi: [10.1088/0004-637X/809/2/123](https://doi.org/10.1088/0004-637X/809/2/123)

Iani, E., Rinaldi, P., Caputi, K. I., et al. 2024, arXiv e-prints, arXiv:2406.18207, doi: [10.48550/arXiv.2406.18207](https://doi.org/10.48550/arXiv.2406.18207)

Izotov, Y. I., Guseva, N. G., Fricke, K. J., & Henkel, C. 2015, *MNRAS*, 451, 2251, doi: [10.1093/mnras/stv1115](https://doi.org/10.1093/mnras/stv1115)

Izotov, Y. I., Guseva, N. G., Fricke, K. J., et al. 2021a, *A&A*, 646, A138, doi: [10.1051/0004-6361/202039772](https://doi.org/10.1051/0004-6361/202039772)

Izotov, Y. I., Guseva, N. G., & Thuan, T. X. 2011, *ApJ*, 728, 161, doi: [10.1088/0004-637X/728/2/161](https://doi.org/10.1088/0004-637X/728/2/161)

Izotov, Y. I., Orlitov  , I., Schaerer, D., et al. 2016a, *Nature*, 529, 178, doi: [10.1038/nature16456](https://doi.org/10.1038/nature16456)

Izotov, Y. I., Schaerer, D., Thuan, T. X., et al. 2016b, *MNRAS*, 461, 3683, doi: [10.1093/mnras/stw1205](https://doi.org/10.1093/mnras/stw1205)

Izotov, Y. I., Schaerer, D., Worseck, G., et al. 2018, *MNRAS*, 474, 4514, doi: [10.1093/mnras/stx3115](https://doi.org/10.1093/mnras/stx3115)

Izotov, Y. I., Thuan, T. X., Guseva, N. G., et al. 2024, *MNRAS*, 527, 281, doi: [10.1093/mnras/stad3151](https://doi.org/10.1093/mnras/stad3151)

Izotov, Y. I., Worseck, G., Schaerer, D., et al. 2021b, *MNRAS*, 503, 1734, doi: [10.1093/mnras/stab612](https://doi.org/10.1093/mnras/stab612)

Jarrett, T. H., Cohen, M., Masci, F., et al. 2011, *ApJ*, 735, 112, doi: [10.1088/0004-637X/735/2/112](https://doi.org/10.1088/0004-637X/735/2/112)

Jaskot, A. E., Dowd, T., Oey, M. S., Scarlata, C., & McKinney, J. 2019, *ApJ*, 885, 96, doi: [10.3847/1538-4357/ab3d3b](https://doi.org/10.3847/1538-4357/ab3d3b)

Kauffmann, G., Heckman, T. M., Tremonti, C., et al. 2003, *MNRAS*, 346, 1055, doi: [10.1111/j.1365-2966.2003.07154.x](https://doi.org/10.1111/j.1365-2966.2003.07154.x)

Kewley, L. J., Dopita, M. A., Sutherland, R. S., Heisler, C. A., & Trevena, J. 2001, *ApJ*, 556, 121, doi: [10.1086/321545](https://doi.org/10.1086/321545)

Kewley, L. J., Groves, B., Kauffmann, G., & Heckman, T. 2006, *MNRAS*, 372, 961, doi: [10.1111/j.1365-2966.2006.10859.x](https://doi.org/10.1111/j.1365-2966.2006.10859.x)

Kim, K., Malhotra, S., Rhoads, J. E., Butler, N. R., & Yang, H. 2020, *ApJ*, 893, 134, doi: [10.3847/1538-4357/ab7895](https://doi.org/10.3847/1538-4357/ab7895)

Kocevski, D. D., Onoue, M., Inayoshi, K., et al. 2023, *ApJL*, 954, L4, doi: [10.3847/2041-8213/ace5a0](https://doi.org/10.3847/2041-8213/ace5a0)

Kocevski, D. D., Finkelstein, S. L., Barro, G., et al. 2024, arXiv e-prints, arXiv:2404.03576, doi: [10.48550/arXiv.2404.03576](https://doi.org/10.48550/arXiv.2404.03576)

Kokorev, V., Fujimoto, S., Labbe, I., et al. 2023, *ApJL*, 957, L7, doi: [10.3847/2041-8213/ad037a](https://doi.org/10.3847/2041-8213/ad037a)

Labbe, I., Greene, J. E., Bezanson, R., et al. 2023, arXiv e-prints, arXiv:2306.07320, doi: [10.48550/arXiv.2306.07320](https://doi.org/10.48550/arXiv.2306.07320)

Leitet, E., Bergvall, N., Hayes, M., Linn  , S., & Zackrisson, E. 2013, *A&A*, 553, A106, doi: [10.1051/0004-6361/201118370](https://doi.org/10.1051/0004-6361/201118370)

Leitherer, C., Hernandez, S., Lee, J. C., & Oey, M. S. 2016, *ApJ*, 823, 64, doi: [10.3847/0004-637X/823/1/64](https://doi.org/10.3847/0004-637X/823/1/64)

Lin, R., Zheng, Z.-Y., Hu, W., et al. 2022, *ApJ*, 940, 35, doi: [10.3847/1538-4357/ac9232](https://doi.org/10.3847/1538-4357/ac9232)

Lin, R., Zheng, Z.-Y., Yuan, F., et al. 2024, *SCIENCE CHINA Physics, Mechanics & Astronomy*, 67, 109811, doi: [10.1007/s11433-024-2412-3](https://doi.org/10.1007/s11433-024-2412-3)

Maiolino, R., Scholtz, J., Curtis-Lake, E., et al. 2023, arXiv e-prints, arXiv:2308.01230, doi: [10.48550/arXiv.2308.01230](https://doi.org/10.48550/arXiv.2308.01230)

Maiolino, R., Scholtz, J., Witstok, J., et al. 2024, *Nature*, 627, 59, doi: [10.1038/s41586-024-07052-5](https://doi.org/10.1038/s41586-024-07052-5)

Matthee, J., Mackenzie, R., Simcoe, R. A., et al. 2023, *ApJ*, 950, 67, doi: [10.3847/1538-4357/acc846](https://doi.org/10.3847/1538-4357/acc846)

Matthee, J., Naidu, R. P., Brammer, G., et al. 2024, *ApJ*, 963, 129, doi: [10.3847/1538-4357/ad2345](https://doi.org/10.3847/1538-4357/ad2345)

McLure, R. J., & Dunlop, J. S. 2004, *MNRAS*, 352, 1390, doi: [10.1111/j.1365-2966.2004.08034.x](https://doi.org/10.1111/j.1365-2966.2004.08034.x)

Mezcua, M. 2017, *International Journal of Modern Physics D*, 26, 1730021, doi: [10.1142/S021827181730021X](https://doi.org/10.1142/S021827181730021X)

Mezcua, M., Pacucci, F., Suh, H., Siudek, M., & Natarajan, P. 2024, *ApJL*, 966, L30, doi: [10.3847/2041-8213/ad3c2a](https://doi.org/10.3847/2041-8213/ad3c2a)

Mezcua, M., Siudek, M., Suh, H., et al. 2023, *ApJL*, 943, L5, doi: [10.3847/2041-8213/aca25](https://doi.org/10.3847/2041-8213/aca25)

Noll, S., Burgarella, D., Giovannoli, E., et al. 2009, *A&A*, 507, 1793, doi: [10.1051/0004-6361/200912497](https://doi.org/10.1051/0004-6361/200912497)

Pacucci, F., Nguyen, B., Carniani, S., Maiolino, R., & Fan, X. 2023, *ApJL*, 957, L3, doi: [10.3847/2041-8213/ad0158](https://doi.org/10.3847/2041-8213/ad0158)

Rhoads, J. E., Wold, I. G. B., Harish, S., et al. 2023, *ApJL*, 942, L14, doi: [10.3847/2041-8213/acaaf](https://doi.org/10.3847/2041-8213/acaaf)

Schaerer, D., Marques-Chaves, R., Barrufet, L., et al. 2022, *A&A*, 665, L4, doi: [10.1051/0004-6361/202244556](https://doi.org/10.1051/0004-6361/202244556)

Stone, M. A., Lyu, J., Rieke, G. H., & Alberts, S. 2023, *ApJ*, 953, 180, doi: [10.3847/1538-4357/acebe0](https://doi.org/10.3847/1538-4357/acebe0)

Sun, F., Egami, E., Pirzkal, N., et al. 2023, *ApJ*, 953, 53, doi: [10.3847/1538-4357/acd53c](https://doi.org/10.3847/1538-4357/acd53c)

Übler, H., Maiolino, R., Curtis-Lake, E., et al. 2023, *A&A*, 677, A145, doi: [10.1051/0004-6361/202346137](https://doi.org/10.1051/0004-6361/202346137)

Wang, B., Heckman, T. M., Leitherer, C., et al. 2019, *ApJ*, 885, 57, doi: [10.3847/1538-4357/ab418f](https://doi.org/10.3847/1538-4357/ab418f)

Wang, L., Hu, M., Wang, L., et al. 2024, *Nature Astronomy*, 8, 504, doi: [10.1038/s41550-024-02197-9](https://doi.org/10.1038/s41550-024-02197-9)

Withers, S., Muzzin, A., Ravindranath, S., et al. 2023, *ApJL*, 958, L14, doi: [10.3847/2041-8213/ad01c0](https://doi.org/10.3847/2041-8213/ad01c0)

Woo, J.-H., Yoon, Y., Park, S., Park, D., & Kim, S. C. 2015, *ApJ*, 801, 38, doi: [10.1088/0004-637X/801/1/38](https://doi.org/10.1088/0004-637X/801/1/38)

Yang, H., Malhotra, S., Gronke, M., et al. 2016, *ApJ*, 820, 130, doi: [10.3847/0004-637X/820/2/130](https://doi.org/10.3847/0004-637X/820/2/130)

Yang, Y., Baade, D., Hoeflich, P., et al. 2023, *MNRAS*, 519, 1618, doi: [10.1093/mnras/stac3477](https://doi.org/10.1093/mnras/stac3477)

Yue, M., Eilers, A.-C., Simcoe, R. A., et al. 2024, *ApJ*, 966, 176, doi: [10.3847/1538-4357/ad3914](https://doi.org/10.3847/1538-4357/ad3914)

Zhang, Z., Jiang, L., Liu, W., & Ho, L. C. 2024, arXiv e-prints, arXiv:2411.02729, doi: [10.48550/arXiv.2411.02729](https://doi.org/10.48550/arXiv.2411.02729)

Zhuang, M.-Y., & Ho, L. C. 2023, *Nature Astronomy*, 7, 1376, doi: [10.1038/s41550-023-02051-4](https://doi.org/10.1038/s41550-023-02051-4)